■ REVIEW

The Extracellular Space in the CNS: Its Regulation, Volume and Geometry in Normal and Pathological Neuronal Function

EVA SYKOVÁ
Department of Cellular Neurophysiology
Institute of Experimental Medicine
Academy of Sciences of the Czech Republic
Prague

Changes in extracellular space (ECS) composition and geometry are a consequence of neuronal activity and of glial K^+, pH, and amino acids homeostasis. They accompany the phenomena of repetitive neuronal activity and also occur as a result of seizures, anoxia, injury, and many other pathological states in the CNS, and they may significantly affect signal transmission in the CNS. Activity-related, or CNS damage-related ionic changes and release of amino acids result in fast, pulsatile, and long-term cellular (particularly glial) swelling. Cellular swelling is compensated for by ECS volume shrinkage and by a decrease in the apparent diffusion coefficients of neuroactive substances diffusing in the ECS. Movement of substances is hindered in the narrower clefts, but presumably also because of the crowding of molecules of the ECS matrix and/or by the swelling of the fine glial processes that form diffusional barriers. This can either increase efficacy of synaptic and nonsynaptic transmission by greater accumulation of substances or induce damage to nerve cells if these substances reach toxic concentrations. NEUROSCIENTIST 3:28–41, 1997

KEY WORDS *Apparent diffusion coefficient, Diffusion, Extracellular volume, Glia, Potassium, pH*

Cellular elements and blood vessels fill ~80% of the total CNS tissue volume, and the remaining portion (15%–25 %) is the extracellular space (ECS). The ECS is the microenvironment of the nerve cells. It includes ions, transmitters, metabolites, peptides, neurohormones, and other neuroactive substances and molecules of the extracellular matrix (ECM), and it directly or indirectly affects neuronal and glial cell functions. In addition, the ECS is an important communication channel (1–6). Populations of neurons can interact both by synapses and by diffusion of ions and neurotransmitters in the ECS. Because glial cells do not have synapses, their communication with neurons is mediated by the diffusion of ions and neuroactive substances in the ECS. In this review, I shall describe the dynamic changes in ECS ionic composition, volume, and geometry that accompany neuronal activity, glial development and proliferation, ageing, and some brain pathological states, and point to their functional significance.

ECS ionic changes resulting from transmembrane ionic shifts during neuronal activity depolarize neighboring neurons and glial cells, enhance or depress their excitability, and affect ion channel permeability (2, 7–9). These ionic changes may also lead to the synchronization of neuronal activity and stimulate glial cell function. Neurons and glia also release transmitters and various other neuroactive substances into the ECS. Substances released nonsynaptically diffuse through the ECS and bind to extrasynaptic, usually high-affinity, binding sites located on neurons, axons, and glial cells. This type of nonsynaptic transmission can be called "diffusion transmission" (neuroactive substances diffuse through the ECS) or "volume transmission" (neuroactive substances move through the volume of the ECS) (3). Neuroactive substances can diffuse through the ECS to target neurons, glial cells, or capillaries. This mode of communication without synapses can function between neurons (even those far distant from release sites), as well as between neurons and glial cells, and may provide a mechanism of long-range information processing in functions, such as vigilance, sleep, chronic pain, hunger, depression, or plastic changes and memory formation. The size and irregular geometry of diffusion channels in the ECS (the so-called tortuosity; see also below) substantially affect the movement of various neuroactive substances in the CNS (Figs. 1 and 2) and, thereby, modulate neuronal signaling and neuron-glia communication. Changes in the ECS diffusion parameters may, therefore, result in impairment of the signal transmission and contribute to functional deficits and to neuronal damage.

Dr. Syková's research is supported by grants GA CR 309/94/1107, GA CR 309/96/0884, GACR 460/321, IGA MZ 3423–3, and U.S.-Czech Science and Technology Program Award 92048.

Eva Syková, M.D., D.Sc., Department of Cellular Neurophysiology, Institute of Experimental Medicine AS CR, Vídeňská 1083, 142 20 Prague 4, Czech Republic.

ISSN 1073-8584

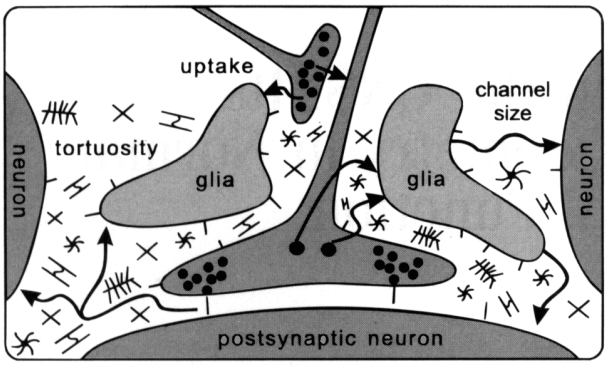

Fig. 1. Schematic of CNS architecture. The CNS architecture is composed of neurons, axons, glial cells, cellular processes, molecules of the extracellular matrix, and intercellular channels between the cells. The architecture affects movement (diffusion) of substances in the brain, which is critically dependent on channel size, extracelluar space tortuosity (λ), and cellular uptake.

ECS Chemical Composition

The solution in the ECS is not a simple salt solution. It has become apparent that long chain polyelectrolytes, either attached or unattached to cellular membranes, are present in the ECS, which also contains some glycosaminoglycans (e.g., hyaluronate), glycoproteins, and proteoglycans that constitute the ECM. Various ECM molecules and adhesion molecules have also been described, e.g., fibronectin, tanescin, and laminin (10), the content of which can dynamically change during development, aging, wound healing, and many pathological processes. The ECM molecules are produced by both neurons and glia. These molecules have been suggested to cordon off distinct functional units in the CNS (groups of neurons, axon tracts, and nuclear groups). As shown in Figure 1, these large molecules can slow down the movement (diffusion) of various neuroactive substances through the ECS. More importantly, these molecules can hinder diffusion of molecules so that they are confined to certain places, while the diffusion to other brain regions will be facilitated.

In the mammalian CNS, the average ionic constituents of the ECS are basically the same as in the cerebrospinal fluid: ~141 mM Na^+, 124 mM Cl^-, 3 mM K^+, 121 mM HCO_3^-, 1.2 mM Ca^{2+}, and ~2.5 mM Mg^{2+}. However, in vivo measurements with ion-selective microelectrodes (Box 1) have revealed local changes in ECS ionic composition resulting from neuronal activity. The local change in ion activity is localized to areas of high spontaneous activity (Fig. 3) (11, 12) or in areas being activated by adequate stimuli, e.g., tactile, visual, auditory, taste aversive, and painful stimuli (13–17). Other important chemical components of the ECS are substances involved in metabolism, particularly glucose and dissolved gases (O_2 and CO_2). The presence of HCO_3^- and CO_2 forms a powerful buffering system that controls extracellular and intracellular pH. The ECS also contains free radical scavengers, such as ascorbate and glutathione, which may counteract some potentially lethal products of oxygen metabolism. In addition, the ECS contains amino acids like glutamate and aspartate; catecholamines; indolamines, such as dopamine and serotonin; various opioid peptides; NO; and growth hormones. Transmitters in the ECS can bind to extrasynaptically located high-affinity binding sites on neurons and glia.

ECS Volume and Geometry: Diffusion Parameters, Inhomogeneity, and Anisotropy

The idea of nonsynaptic transmission between cells has gained support in many studies (1, 4, 6, 20). The diffusion of substances released from neurons or glial cells into narrow ECS is hindered by the size of the channels between cells, the presence of membranes, fine processes, macromolecules of the ECM, charged molecules, and also the cellular uptake or degradation of these substances by enzymes (Fig. 1). Diffusion in the ECS obeys Fick's law, albeit subject to important modifications (Fig. 2). First, diffusion is constrained by the restricted volume of the tissue available for diffusing particles, i.e., by the ECS volume fraction (α), which is the ratio between the volume of the ECS and total tissue volume. It is now clear that the ECS in adult brain amounts to ~20% of the total brain volume, i.e., $\alpha = 0.2$. The second modification to Fick's law is that the free diffusion coefficient, D, is reduced by the tortuosity factor (λ). ECS tortuosity is defined as $\lambda = (D/ADC)^{0.5}$, where ADC is the apparent diffusion coefficient in the brain and D is a free diffusion coefficient. As a result of tortuosity, D is reduced to an apparent diffusion coefficient $ADC = D/\lambda^2$. Thus, any substance diffusing in the ECS is hindered by membrane obstructions, glycoproteins, macromolecules of the ECM, charged molecules, and fine neuronal and glial cell processes. Third, substances released into the ECS are transported across membranes by nonspecific concentration-dependent uptake (k'). In many cases, however, these substances are transported by energy-dependent uptake systems that obey nonlinear kinetics (21). When these three factors (α, λ and k') are incorporated into Fick's law, diffusion in the CNS is described fairly satisfactorily (Box 2) (22).

To describe the diffusion constraints of the neuroactive substances and their dynamic changes in vivo, the diffusion parameters of the ECS are studied using the real-time inotophoretic method (22) described in Box 2. This method allows us to follow the diffusion of extracellular markers applied by iontophoresis (Fig. 4). The absolute values of the ECS volume, ADCs, tortuosity, and nonspecific cellular uptake can be obtained both in vivo or in vitro, during physiological and in pathological states. To date, other methods used to study ECS volume and geometry in vivo have been less comprehensive because they can give only either relative changes in ECS volume—these methods include light scattering (23),

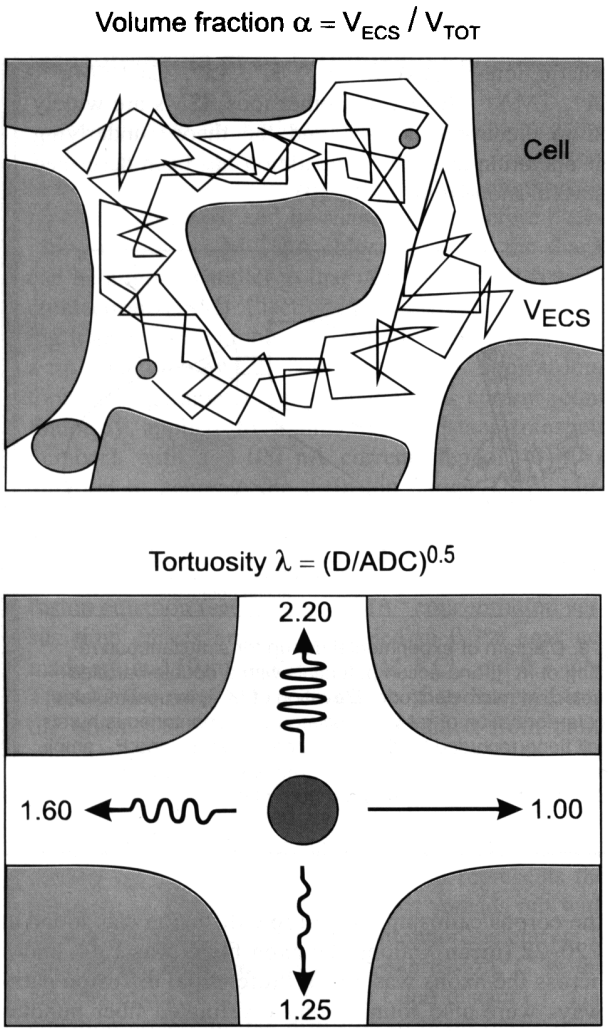

Fig. 2. Concept of extracellular space (ECS) volume fraction (α) and tortuosity (λ). V_{ECS}, volume of the ECS; V_{TOT}, total brain (spinal cord) volume; D, free diffusion coefficient; ADC, apparent diffusion coefficient of a substance in nervous tissue. Small substances move in the ECS by Brownian motion. Large substances still migrate through ECS but are more hindered by narrow interstices. Values of λ correspond to TMA^+ diffusion: 1.00—free solution, 1.60—adult rat cortex, 1.25—severe edema, 2.20—severe anoxia/ischemia. For further details, see text.

measurements of tissue resistance (24–26), and measurement of ADCs of molecules tagged with fluorescent dye and followed by optical imaging (27)—or changes in ADC of water (ADC_w) measured by diffusion-weighted NMR (28–31). The optical methods can only be used in vitro, particularly on brain slices. Diffusion-weighted NMR methods give information about the water diffusion coefficient, but the relationship between water movement, diffusion ADC_w maps, and the changes in cell volume and ECS diffusion parameters (ECS volume fraction and tortuosity) is not yet well understood. Relatively small changes in water movement might account for changes in intracellular and extracellular space volume.

Neuroactive substances released constantly into the ECS will accumulate in this limited volume more rapidly than in free solution. Tortuosity (which is absent in free medium) also causes greater and more rapid accumulation of released substances. CNS tortuosity reduces the diffusion coefficient for small molecules by a factor of ~2.5 in many CNS regions. Larger molecules (with relative molecular mass above 10 kDa), have a smaller diffusion coefficient than small molecules and are significantly more hindered in their diffusion; therefore, they exhibit larger tortuosity (32, 33). Even large proteins, e.g., negatively charged globular proteins, such as bovine serum albumin (66 kDa) or dextrans of 70 kDa, still migrate through narrow interstices of brain slices (27, 34).

Values in Box 3 show that the ECS diffusion parameters are different in different parts of the CNS. For example, it has been recognized that the TMA^+ diffusion parameters in the sensorimotor cortex of young adult rats in vivo are heterogeneous (35). The mean volume fraction gradually increases from $\alpha = 0.19$ in cortical layer II to $\alpha = 0.23$ in cortical layer VI. In subcortical white matter (corpus callosum), the volume fraction is always lower than in layer VI, often 0.19–0.20 (35). These typical differences are apparent in each individual animal. The mean tortuosity values are typically in the range of 1.51–1.65, and k' values vary between 3.3–6.3 $\times 10^{-3}$ s^{-1}. Significantly lower α values than in the cortex and corpus callosum have been found in the rat hippocampus in vivo (36), as well as in hippocampal slices (37, 38) (Box 3). Exceptionally low values of α were found in area CA1 (~0.12 in stratum pyramidale and 0.16 in stratum radiatum), whereas in CA3 and dentate gyrus α values were considerably higher, ~0.16–0.19. One explanation for this may be that the intercellular channels of the ECS are not homogeneous, i.e., that sizes vary in diameter. It is not clear whether the intercellular channels of the ECS in certain anatomical regions are different but homogeneous, or whether the average channel size is smaller or larger. Older morphological studies revealed the existence of much narrower channels (apparently artificially too narrow because of histological fixation) and much larger spaces, or so-called "lakes" (45, 46), which may only allow the diffusion of larger substances. Significant differences in various brain regions have also been found in tortuosity, showing that the local architecture is significantly different. There is also a heterogeneity in the spinal cord (Box 3), with the mean values of the volume fraction highest in the ventral horn ($\alpha = 0.23$) and lowest in the white matter ($\alpha = 0.18$) (40).

Is there some degree of anisotropy in brain tissue? Isotropy is defined as a state of constant λ in any direction from a point source, whereas anisotropy indicates a difference in λ in different axes. To test for anisotropy, the ECS diffusion parameters are measured in three orthogonal axes—x, y, and z. Anisotropic diffusion can

Box 1: Ion-selective Microelectrodes

An ion-selective microelectrode (ISM) is a miniaturized potentiometric sensor that consists of a liquid membrane (liquid ion-exchanger, ion-carrier) placed in the tip of a glass micropipette. When introduced into a tissue or calibration solution where ionic activity is to be measured, a Nernst potential develops across the ion-exchanger membrane, i.e., one measures a potential that changes logarithmically with the activity of the ion for which the ion-exchanger is selective. However, when the microelectrode is inserted into neural tissue, it records not only electrical potential differences generated by free ion concentrations, but all types of electrical activity, including membrane, field, action, and synaptic potentials. These disturbing factors can be abolished if a reference electrode is in the immediate vicinity of the tip of the ISM. This requirement is best fulfilled by a double-barreled microelectrode (Fig. 3) that has a liquid ion-exchanger in one channel, while the other channel serves as the reference microelectrode and is, therefore, filled with saline or some other indifferent solution. Because the reference microelectrode also records electrical activity in the tissue, the signal from it is used to cancel out the undesired component. We now have at our disposal ion-exchangers (natural and synthetic ionophores) for H^+, K^+, Li^+, Ca^{2+}, Mg^{2+}, TEA^+, TMA^+, HCO_3^- and other ions. ISMs are widely used in electrophysiology, and the theory underlying their operation and their preparation has been described in several monographs (18, 19).

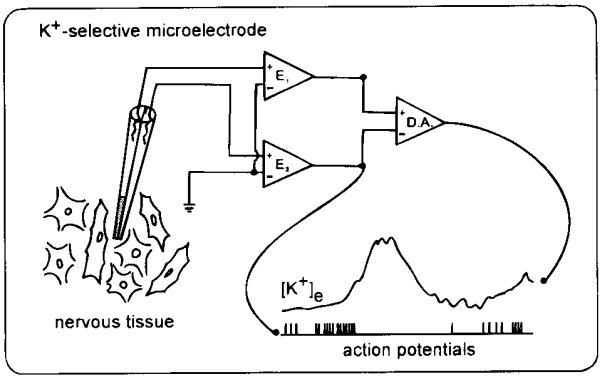

Fig. 3. Diagram of experimental set-up for simultaneous recording of $[K^+]_e$ and action potentials with a double-barreled K^+-selective microelectrode. Elevation of $[K^+]_e$ in unstimulated reticular formation of rat is associated with spontaneous bursts of cell firing recorded by the reference barrel. E_1 and E_2, amplifiers; D.A., differential amplifier for measurements with ion-selective microelectrodes. Adapted from (11).

channel the migration of substances in the ECS (preferred diffusion in one direction, e.g., along the axons) and may, therefore, account for a certain degree of specificity of the diffusion transmission. The structure of cells and axons can channel the migration of substances in the ECS, and this could be a mechanism for a specificity of diffusion transmission of signals. Indeed, anisotropic diffusion was described using the "TMA^+-method" in the molecular layer of the cerebellum (47). Because the molecular and granular layers of the cerebellum have distinct diffusion characteristics, the extracellular molecular traffic will be different in the two regions. The anisotropy of the white matter and molecular layer of the cerebellum could enable different modes of diffusion transmission in these regions.

Diffusion parameters are substantially different in the myelinated and unmyelinated white matter of the rat during postnatal development (48). Isotropic diffusion was found in corpus callosum and spinal cord white matter of rats with incomplete myelination. In myelinated spinal cord and corpus callosum, the tortuosity is higher (the apparent diffusion coefficient is lower) when TMA^+ diffuses across the axons than when it diffuses along the fibers. In white matter of the rat spinal cord at postnatal day 12–14 (P12–14), mean λ along the axon fibers was 1.36, whereas λ across the axons was 1.82. At P7, diffusion was still isotropic. In the corpus callosum, anisotropic diffusion was found at P20–22 (mean λ along the axon fibers was 1.44, and λ across the axons was 1.69). Preferential diffusion pathways were also found along myelinated fiber bundles in the living brain using Texas Red-labeled dextran injected into neostriatum of adult rats (49). These results confirm the hypothesis that there are preferential diffusion pathways of chemical signals along the myelinated fibers in white matter tracts.

Diffusion images of water have been obtained recently by MRI (50). Measuring water diffusion in vivo permits noninvasive observation of tissue architecture and microstructure. As with TMA^+ diffusion, the apparent diffusion coefficient of water (ADC_W) is lower in brain than in free water (51) because of cell membranes, axons, and macromolecules of ECM—all important diffusion barriers in CNS. Using MRI, evidence of anisotropic diffusion in white matter was found in cat brain (52), as well as in human brain (53). The measured ADC_W values are significantly smaller when the gradient pulses of the diffusion imaging sequence are perpendicular to the direction in which the myelinated axons run, although water diffuses with a measurable rate across myelinated axons. Therefore, not only the diffusion of large molecules, such as TMA^+ or dextrans, but even the diffusion of water, are prevented by the presence of the myelin sheets.

Box 2: Real-time Iontophoretic Method for Measurements of ECS Diffusion Parameters

Ion-selective microelectrodes are used to measure TEA^+,TMA^+, choline, or AsF^- diffusion parameters in ECS. For diffusion measurements, the iontophoresis pipette is prepared, and its shank is bent before backfilling it with ~1 M TMA chloride, so that the shank can be aligned parallel to that of the ion-selective microelectrode (ISM). Electrode arrays are made by gluing together an iontophoresis pipette and an ISM with a tip separation of 130–200 μm (Fig. 4). Typical iontophoresis parameters are +20 nA bias current (continuously applied to maintain a constant transport number), with a +100 nA current step of 40–80 s duration to generate the diffusion curve. TMA^+ diffusion curves are captured on a digital oscilloscope and then transferred to a computer, where they are analyzed by fitting the data to a solution of the diffusion equation (see below). TMA^+ concentration versus time curves are first recorded in 0.3% agar gel made up in 150 mM NaCl, 3 mM KCl, and 0.3 mM TMA^+. The array of electrodes is then lowered into the brain. The diffusion curves obtained from brain are analyzed to yield λ, α, and the nonspecific, concentration-dependent uptake term, k' (s^{-1}). These three parameters are extracted by a nonlinear curve-fitting simplex algorithm operating on the diffusion curve described by Equation [1] below, which represents the behavior of TMA^+, assuming that it spreads out with spherical symmetry, when the iontophoresis current is applied for duration S. In this expression, C is the concentration of the ion at time t and distance r. The equation governing the diffusion in brain tissue is:

$C = G(t)$ $\quad t < S$, for the rising phase of the curve

$C = G(t) - G(t\text{-}S)$ $\quad t > S$, for the falling phase of the curve.

The function G(u) is evaluated by substituting t or t-S for u in the following equation (22):

$$G(u) = (Q\lambda^2/8\pi D\alpha r)\{\exp[r\lambda(k'/D)^{1/2}]\,\mathrm{erfc}[r\lambda/2(Du)^{1/2} + (k'u)^{1/2}] + \exp[-r\lambda(k'/D)^{1/2}]\,\mathrm{erfc}[r\lambda/2(Du)^{1/2} - (k'u)^{1/2}]\} \quad [1]$$

The quantity of TMA^+ or TEA^+ delivered to the tissue per second is Q = In/zF, where I is the step increase in current applied to the iontophoresis electrode, n is the transport number, z is the number of charges associated with the substance iontophoresed (+ 1 for TMA^+ or TEA^+), and F is Faraday's electrochemical equivalent. The function "erfc" is the complementary error function. When the experimental medium is agar, by definition, α = 1 = λ and k' = 0, and the parameters n and D are extracted by the curve fitting. Knowing n and D, the parameters α, λ, and k' can be obtained when the experiment is repeated in the neural tissue.

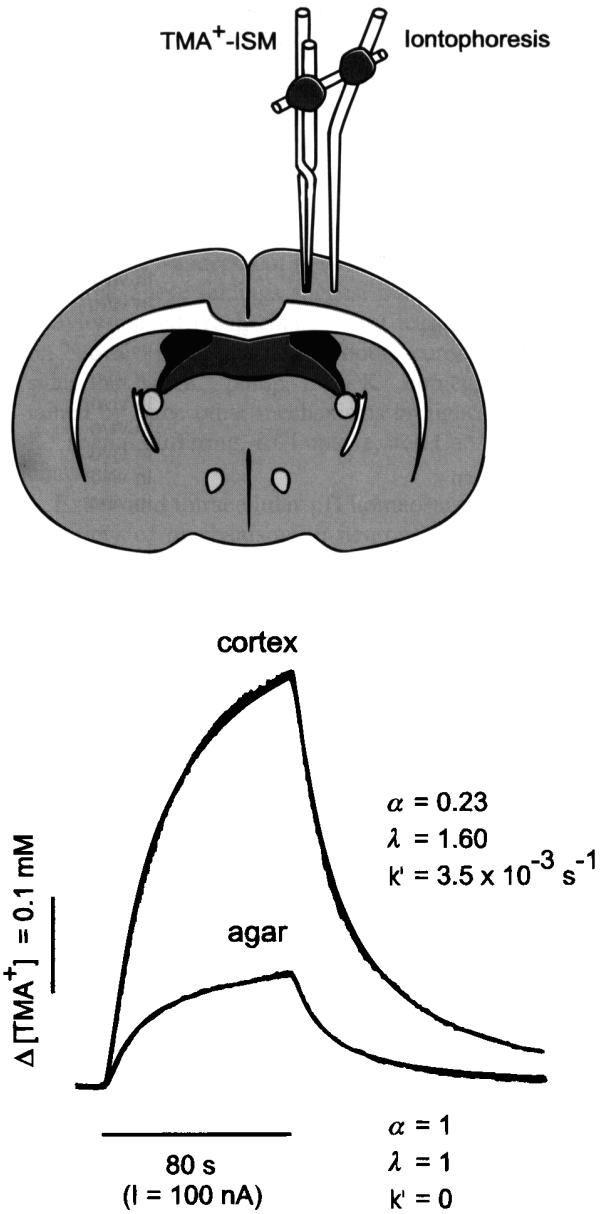

Fig. 4. Experimental set-up, TMA^+ diffusion curves and typical ECS diffusion parameters α (volume fraction), λ (tortuosity) and k' (nonspecific TMA^+ uptake). *Left*, schema of the experimental arrangement. A TMA^+-selective, double-barreled, ion-selective microelectrode (ISM) was glued to a bent iontophoresis microelectrode. The separation between electrode tips was 130–200 μm. *Right*, typical records obtained in agar gel and in rat cortex. Measurements in agar, where α = 1 = λ, and k' = 0 (free diffusion values) were analyzed to yield the TMA^+ free diffusion coefficient (D) and the iontophoretic electrode transport number (n). The diffusion curve was then recorded with the same microelectrode array in rat cortex (layer V), and the calculated diffusion parameters α, λ, and k' are shown with the record. The concentration scale is linear, and the theoretical (*blue*) diffusion curve (Expression 1) is superimposed on each data curve (*black*). When the electrode array was inserted into the lamina V of the adult rat cortex and an iontophoretic current was applied, the resulting increase in concentration was much larger in the brain than in agar, apparently because of smaller volume fraction.

Box 3: Values of Volume fraction (α) and Tortuosity (λ) Obtained with Real-Time Iontophoretic Method in CNS of the Adult Rat

Region	Status	α	λ	References
Spinal cord, dorsal horn	In vivo	0.20	1.62	(39)
	In vivo	0.21	1.55	(40)
Intermediate region	In vivo	0.22	1.54	(40)
Ventral horn	In vivo	0.23	1.46	(40)
White matter	In vivo	0.18	1.56[a]	(40)
Neocortex	In vivo	0.18	1.57	(41)
	In vivo	0.18	1.40[b]	(42)
	In vitro	0.18	1.62	(38)
Sensorimotor cortex				
Layer II	In vivo	0.19	1.51	(35)
Layer III	In vivo	0.20	1.63	(35)
Layer IV	In vivo	0.21	1.59	(35)
Layer V	In vivo	0.22	1.62	(35)
Layer VI	In vivo	0.23	1.65	(35)
Corpus callosum	In vivo	0.20	1.55[a]	(35)
Neostriatum	In vitro	0.21	1.54	(43)
Hippocampus				
CA1 st. pyramidale	In vivo	0.12	1.34	(36, 44)
	In vitro	0.12; 0.14	1.67; 1.50	(37, 38)
CA1 st. radiatum	In vivo	0.16	1.44	(36, 44)
	In vitro	0.13	1.71	(37)
CA3 st. pyramidale	In vivo	0.19	1.53	(36, 44)
	In vitro	0.18; 0.20	1.83[b]; 1.57	(37, 38)
CA3 st. radiatum	In vivo	0.16	1.41	(36, 44)
	In vitro	0.16	1.71[b]	(37)
Cerebellum, molecular layer	In vivo	0.21	1.55[a]	(22)

[a]Measurements did not take anisotropy into account.
[b]Measurements did not take nonspecific TMA^+/TEA^+ uptake into account.

Activity-related Ionic and Volume Changes in the ECS: Their Origin, Homeostasis, and Physiological Role

An activity-related increase in extracellular K^+ activity ($[K^+]_e$), alkaline and acid shifts in pH_e, and a decrease in extracellular Ca^+ concentration ($[Ca^{2+}]_e$) have been found to accompany neuronal activity in a variety of animals and brain regions in vivo, as well as in vitro (2, 4, 8). Dynamic changes in $[K^+]_e$ have been recorded in the immediate vicinity of individual neurons in the mesencephalic reticular formation (MRF) of the rat. MRF is recognized as a structure with high spontaneous activity level. During a burst of spontaneous action potentials, $[K^+]_e$ steadily increases by as much as 0.2 mM (11). The neurons start to fire again when the K^+ elevation returns to the "resting" K^+ baseline (Fig. 3), suggesting that accumulation of K^+ in the ECS blocks spontaneous activity.

Most frequently, neuronal activity results in an increase in $[K^+]_e$, a decrease in $[Ca^{++}]_e$, and a rapid extracellular alkaline shift, followed by a slower but longer-lasting acid shift (11, 16, 54). After sustained adequate stimulation of the afferent input or after repetitive electrical stimulation, the ionic transients reach a certain steady state, the so-called "ceiling" level (Fig. 3). The K^+ ceiling level in the mammalian cortex is ~7 mM K^+ (55) and in the mammalian spinal cord, 6–8 mM K^+ (16, 56). The alkaline shifts in mammalian cortex, cerebellum, or spinal cord do not exceed 0.02 pH units, and the acid shifts are ~0.2 pH units (4, 8, 9). For example, after tetanic stimulation of the sciatic nerve (30–100 Hz), the $[K^+]_e$ "ceiling" level in the adult rat or cat spinal cord is attained in 5–8 s, whereas the "ceiling" level of the acid shift is reached in 10–20 s (16, 56). When stimulation is continued beyond this, a gradual decrease of both transients, $[K^+]_e$ and pH_e, occur after the ceiling levels are reached because of homeostatic mechanisms in neurons and glia (Fig. 5).

Adequate stimulation, which includes innocuous stimuli, acute nociceptive stimuli, or peripheral tissue injury of a hind paw, result in activity-related transient K^+ and pH_e changes in the spinal dorsal horn (14, 16). In the visual cortex of cats (13) and in the ectostriatum of chicks (17), a rise in $[K^+]_e$ and pH shifts accompany neuronal activity during stimulation of the receptive field with visual stimuli. Stimulation with pure-tone acoustic stimuli over a frequency range of 500 Hz–25 kHz produces changes of ~1 mM K^+ in the organ of Corti, with the maximal change between supporting cell and inner hair cell (15). The K^+ and pH changes evoked by adequate stimulation are generally of smaller amplitude than those evoked by electrical stimulation, with an increase in $[K^+]_e$

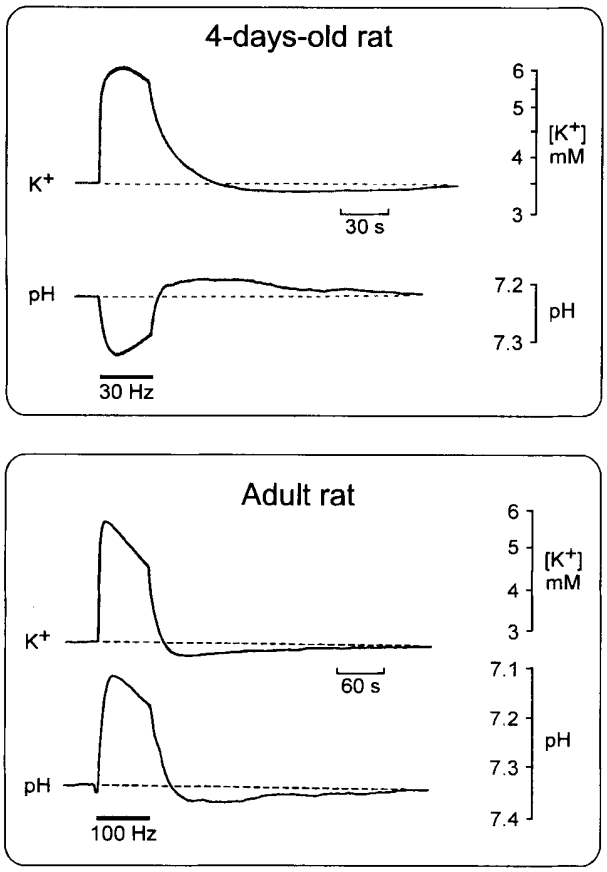

Fig. 5. Stimulation-evoked pH_e and $[K^+]_e$ changes in the spinal dorsal horn of 4-day-old and adult rats. The stimulation of the dorsal root at a frequency of 10 Hz evoked a typical alkaline shift in a 4-day-old pup, accompanied by an increase in $[K^+]_e$. In adult rats, even a stimulation of 100 Hz evoked a smaller increase in $[K^+]_e$. The change in pH_e was biphasic; first a small and fast "initial" alkaline shift occured, which was followed by dominating acid shift. Note the poststimulation undershoots in $[K^+]_e$, as well as in pH_e. Adapted from (4, 54).

of ~1–3 mM and an acid shift of up to ~0.05–0.1 pH units, but they can last longer. For example, after peripheral injury $[K^+]_e$ increase and pH_e decrease in the spinal dorsal horn begin 2–10 min after injury, reach their maximum in 15–40 min, and then persist for >2 h.

Transmembrane ionic fluxes are accompanied by the movement of water and cellular—presumably, particularly glial—swelling. Changes in ECS diffusion parameters (ECS volume decrease, tortuosity increase, and ADC decrease) are the consequence of activity-related transmembrane ionic shifts and cellular swelling. In the spinal cord of the rat or frog, repetitive electrical stimulation results in an ECS volume decrease from ~0.24 to 0.12–0.17, i.e., the ECS volume decreases by as much as 30%–50% (57). The changes in ECS diffusion parameters persist for many minutes or even hours after the stimulation has ceased, suggesting long-term changes in neuronal excitability and neuron-glia communication (Fig. 6).

Mechanisms of the ECS Ionic Homeostasis

Mechanisms for ECS ionic homeostasis have been described in several reviews (2, 4, 8, 58, 59), and, therefore, only a brief summary is given here. K^+, pH, and apparently also volume homeostasis in the CNS are ensured by a variety of mechanisms in both neurons and glia. After returning to the prestimulation $[K^+]_e$ values, a transient decrease in $[K^+]_e$ occurs below the original K^+ baseline, the so-called poststimulation K^+-undershoot (55, 56). This K^+-undershoot is blocked by ouabain or during hypoxia. These findings suggest that the recovery of the activity-related $[K^+]_e$ change is at least partly dependent on Na^+/K^+ pump activity in both neurons and glia. Besides the Na^+/K^+ pump, ECS K^+ homeostasis is maintained by three other mechanisms brought about by glia: K^+ spatial buffering, KCl uptake, and Ca^{++}-activated K^+ channels.

Extra- and intracellular pH homeostasis is ensured by a variety of mechanisms in neurons and glia (4, 8, 9). There is now convincing evidence for the neuronal origin of extracellular alkaline shifts and the glial origin of activity-related acid shifts (54, 60). Substantial differences exist in activity-related pH_e and $[K^+]_e$ changes in adult animals (with completed gliogenesis and glial cell function) and during early postnatal development, presumably because of incomplete glial cell function, apparently because glial maturation and myelination occur postnatally and more slowly than neuronal maturation. In the neonatal rat spinal cord, stimulation-evoked changes in $[K^+]_e$ are much larger than in the adult animal (54). In neonates, ECS alkaline shifts dominate because the acid shift generated by glia is small (Fig. 5). At postnatal day 10, when gliogenesis in rat spinal cord gray matter peaks, the K^+ ceiling level decreases, and stimulation evokes acid shifts of ~0.1–0.2 pH unit, which are preceded by scarcely discernible alkaline shifts, as is also the case in adult rats (Fig. 5 and 6). In addition, stimulation-evoked alkaline shifts are abolished by the blockage of synaptic transmission by Mn^{++} or Mg^{++} (whereas acid shifts are unaffected) (60), by the GABA antagonist picrotoxin, and by glutamate receptor antagonists and channel blockers, such as MK801 (noncompetitive NMDA receptor antagonist and channel blocker) and CNQX (competitive AMPA/kainate receptor antagonist) (60, 61). These results show that glial cells play an important role in buffering activity-related alkaline changes in extracellular pH.

Some of the membrane transport processes regulating intra- and extracellular pH, such as Na^+/H^+ exchange and $Na^+/H^+/Cl^-/HCO_3^-$ cotransport, are present in both neurons and glia; others are specific for neurons (H^+ channels, H^+ or HCO_3^- permeability of the ionic channels opened by GABA or glutamate) or for glia (e.g., the voltage-dependent Na^+-HCO_3^- cotransport and lactate extrusion). The glial cell membrane is also readily permeable to CO_2, which reacts with H_2O to form bicarbonic acid, which, in turn, quickly dissociates into water and protons.

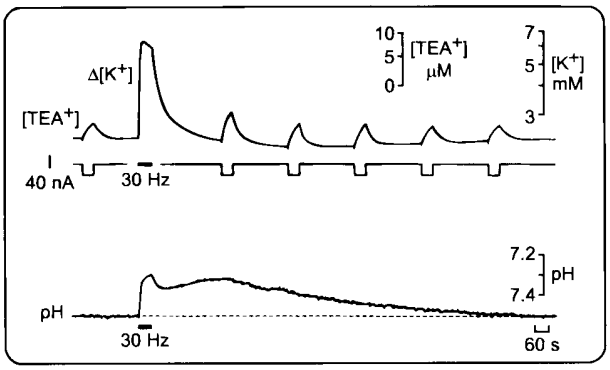

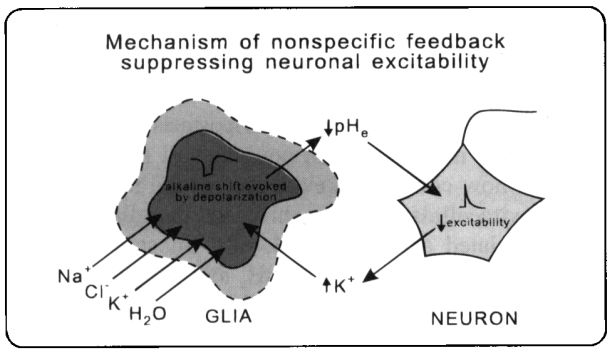

Fig. 6. *Top panel*, effect of repetitive electrical stimulation of dorsal root on ECS volume and pH_e in the dorsal horn of an isolated frog spinal cord. Current (40 nA, bottom recordings) was applied with an iontophoretic pipette filled with TEA^+. Top records show TEA^+ diffusion curves recorded using the method described in Box 2 and change in $[K^+]_e$ (TEA^+ electrode is also sensitive to K^+) induced by repetitive stimulation (30 Hz, 60 s). pH_e: Concomitantly recorded pH_e changes with pH-selective microelectrode. *Bottom panel*, a schematic of the mechanism of nonspecific feedback suppressing neuronal excitability. Active neurons release K^+, which accumulates in the ECS and depolarizes glial cells, causing an alkaline shift in glial pH_i and an acid shift in pH_e. Extracellular acidosis further suppreses neuronal activity. Transmembrane ionic movements results in glial swelling, ECS volume decrease, and, therefore, in the greater accumulation of ions and neuroactive substances in the ECS.

This reaction is catalyzed and sped up by the enzyme carbonic anhydrase (CA), which is present in glia. Some of the membrane transport mechanisms result in alkaline shifts in pH_e (acid loaders), whereas others result in acid shifts in pH_e (acid extruders), but it is evident that acid loaders are dominant in neurons and acid extruders are dominant in glia (4, 8, 9). Extracellular acid shifts are, therefore, a consequence of activity-related extracellular K^+ increase. K^+-induced glial depolarization results in alkaline shift in glial pH_i, which leads to stimulation of classic acid extrusion systems in glial cells. The following nonspecific feedback mechanism suppressing neuronal activity may exist in the CNS (Fig. 6):

- Neuronal activity results in the accumulation of $[K^+]_e$;
- K^+ depolarizes glial cells, and this depolarization induces an alkaline shift in glial pH_i;
- The glial cells, therefore, extrude acid; and
- The acid shifts in pH result in a decrease in the neuronal excitability.

Furthermore, because the ionic movements are always accompanied by water, this feedback mechanism would be amplified by activity-related glial swelling, for which ECS volume shrinkage compensates (Fig. 4), and by increased tortuosity, presumably by the crowding of molecules of the ECS matrix and by the swelling of fine glial processes. This would result in greater accumulation of ions and other neuroactive substances in brain because of hindrance of their diffusion in ECS.

Mechanisms of ECS Volume and Geometry Changes

It is generally accepted that the ECS volume decrease results primarily from astrocytic swelling, although swelling of neurons, particularly of dendrites and axons, also occurs. Activity-related or CNS damage-related ionic changes and release of amino acids result in pulsatile or long-term glial swelling, which leads to a compensatory decrease in the ECS volume and increased tortuosity (i.e., decrease in ADC). In turn, an ECS volume decrease is predicted to result in a greater accumulation of neuroactive substances that can ultimately induce damage to the nerve cells by reaching toxic concentrations. Some mechanisms have been proposed to lead to astrocytic swelling—namely, osmotic imbalance, uptake of extracellular K^+, acid-base changes, glutamate uptake and excitatory amino acid-induced swelling, blockage of Na^+/K^+ pump activity, and accumulation of fatty acids and free radicals (62, 63). For the most part, these mechanisms of swelling have been confirmed primarily in tissue culture, and they were only recently compared with changes in ECS volume and geometry.

Mechanisms of changes in ECS volume and geometry have been studied using the TMA^+ method in the cerebral cortex of the in vivo rat (41), isolated rat spinal cord (64), brain slices (65), and isolated turtle cerebellum (33). The observed mechanisms might be similar to those of cellular swelling, although there are some differences in the effects of cellular swelling on the ECS volume and on the ECS tortuosity. In the in vivo rat studies, acute hypernatremia caused a reduction in ECS volume fraction from 0.18 to 0.10–0.15 and an increase in tortuosity from 1.57 to 1.65, with little change in intracellular volume, demonstrating cellular volume regulation in the intact animal (41). The application of hypotonic solution of physiological saline, with elevated $[Na^+]_e$, or glutamate resulted in a dramatic ECS volume decrease and an ECS tortuosity increase (33, 64). Measurements of ECS volume fraction and water content showed that hypotonic solutions caused water to move from the extracellular to intracellular compartment, whereas hypertonic solutions caused water to move from the intracellular to extracellular compartment, with relatively small changes in total water in both cases (33).

The superfusion of isolated rat spinal cords with solutions containing 10 mM K^+, or low doses of glutamate or glutamate receptors agonists (NMDA or AMPA at 10^{-5} M) was used as a model of changes in ECS diffusion parameters during neuronal activity and stimulation. This resulted in the shrinkage of the ECS by as much as 20%–25% and an increase in λ from ~1.5 to ~1.8. Specific antagonists blocked the effects of NMDA and AMPA. Superfusion with 50 mM K^+ or higher concentrations of glutamate (at 1–10 mM) or the glutamate receptors agonists NMDA or AMPA (at 10^{-4} M) provided a model of changes during pathological events, such as anoxia, ischemia, or injury. Solutions containing 50 mM K^+ induced a decrease in α to as low as 0.04–0.05 and an increase in λ to as high as 2.1–2.2. Application of NMDA or AMPA resulted in a drop in α to 0.04–0.07 and in large increases in λ to as high as 1.85–2.10. Glutamate in relatively high concentrations (1–10 mM) was less effective. Further measurements in the isolated rat spinal cord also revealed that changes of 0.2–0.4 pH units and greater of the superfusing solution led to changes in ECS volume—namely, an alkaline shift in pH causes an ECS volume increase and an acid shift causes an ECS volume decrease (64). The ECS volume changes evoked by all of these swelling-inducing substances were reversible upon superfusion of the spinal cord with physiological solution. In many cases, the ECS volume changes started to recover toward control values during application of swelling-inducing substances, apparently because the cells started to regulate their volume, a phenomenon called regulatory volume decrease.

Role of Glia and Extracellular Macromolecules in the ECS Geometry

It is reasonable to assume that ions, as well as neurotransmitters, released into the ECS during neuronal activity or pathological states interact not only with the postsynaptic and presynaptic membranes, but also with extrasynaptic receptors, including those on glial cells. A stimulation of glial cells may lead to activation of ion channels, second messengers, and intracellular metabolic pathways, and to changes in their volume, accompanied by dynamic variations in the ECS volume, particularly swelling and, possibly, rearrangement of their processes. In addition to their role in maintenance of extracellular ionic homeostasis, glial cells may, thus, by regulating their volume, influence extracellular pathways for neuroactive substances.

Many pathological processes in the CNS are accompanied by loss of cells or neuronal processes, astrogliosis, demyelination, and changes in the ECM, all of which may affect apparent diffusion coefficients of neuroactive substances. Several animal models have been developed to study the changes in ECS diffusion parameters. Brain injury of any kind elicits reactive gliosis, involving both hyperplasia and hypertrophy of astrocytes, which show intense staining for glial fibrillary acidic protein (GFAP). Astrogliosis is also a typical characteristic of cortical stab wounds in rodents (66). The lesion is typically accompanied by a modest ECS volume increase and by substantial increase in tortuosity to mean values of λ ~1.76 (Box 4, Syková, Mazel and Roitbak, unpublished data). Similarly, in grafted neural tissue (e.g., in cortical grafts of fetal tissue) there is severe astrogliosis compared with normal cortex (67). The size of the ECS (α) and surprisingly also λ, were significantly higher in cortical grafts than in host cortex, ~0.35 and 1.79, respectively, as it is also the case in gliotic cortex after stab wounds. Another characteristic feature of grafts is the variability of α and λ. The different values in various depths of grafts correlated with the morphological heterogeneity of graft neuropil. These measurements show that even when the ECS in gliotic tissue or in cortical grafts is larger than in normal cortex, the tortuosity is still higher and the diffusion of chemical signals in such tissue may be hindered. A limited diffusion may also have a negative impact on the viability of grafts in host brains. Compared with host cortex, immunohistochemistry showed myelinated patches and more hypertrophic astrocytes in areas of high λ values, suggesting that more and/or thicker glial cell processes may be the cause of the increased tortuosity. However, changes in the ECM cannot so far be excluded. These studies support the role of glial cell processes as diffusion barriers in the CNS.

The ECM molecules and other large molecules can also affect the tortuosity of the ECS. Their possible effect on changes in TMA^+ diffusion parameters have been studied in rat cortical slices (32, 34) and in rat isolated spinal cord (48). Superfusion of the the slice or spinal cord with a solution containing either 40-kDa or 70-kDa dextran or hyaluronic acid (HA) resulted in a significant increase in λ. In a standard physiological solution, λ was ~1.57, whereas in 1% or 2% solution of 40-kDa or 70-kDa dextran, λ increased to ~1.72–1.77. Application of a 0.1% solution of HA (1.6×10^6 Da) resulted in an increase in λ to ~1.75. The α was unchanged in these experiments, suggesting that these substances had no effect on cellular volume and viability of the preparation. These results suggest that bigger molecules, such as 40- and 70-kDa dextran and HA, may slow down the diffusion of small molecules, such as TMA^+ (74 Da) in ECS.

ECS During Development and Aging

Compared with those of healthy adults, the ECS diffusion parameters significantly differ during postnatal development (35). The ECS volume in the cortex and subcortical white matter (corpus callosum) is about twice as large (α = 0.36–0.46) in the newborn rat as in the adult rat (α = 0.19–0.23), whereas the variations in tortuosity are not statistically significant at any age (Box

Box 4: Mean Values of the ECS Diffusion Parameters during Development, Aging, and Pathological States as Measured by TMA^+-method (all data from rats in vivo).

Status	Region	α	λ	References
Development (P2)	Cortex	0.36–0.41	1.59–1.68	(35)
	Corpus callosum	0.46	1.58	(35)
Aging	Cortex	0.18–0.19	1.52–1.59	(36, 44)
	Corpus callosum	0.15	1.46[a]	(36, 44)
	Hippocampus CA1	0.09	1.36	(36, 44)
Chronic pain	Spinal cord	0.12	—	(54)
Hypoxia	Spinal cord	0.16	1.62	(39)
Terminal anoxia	Spinal cord	0.07	2.20	(39)
	Cortex	0.07	1.63[b]	(42)
		0.06	2.00	(66) (in press)
	Corpus callosum	0.05	2.10[a]	(66) (in press)
Recovery after anoxia	Spinal cord	0.30	1.63	(39)
Hypernatremia	Cortex	0.10–0.15	1.65	(41)
Astrogliosis-stab wounds	Cortex	0.26	1.76	Syková et al. (unpublished).
X-irradiation acute state	Cortex	0.48–0.51	1.42–1.56	(68)
X-irradiation chronic state	Cortex	0.34–0.55	1.56–1.81	(68)
EAE	Spinal cord, dorsal horn	0.28	1.40	(40)
	Spinal cord, ventral horn	0.47	1.48	(40)
	Spinal cord, white matter	0.30	1.48	(40)
Cortical grafts	—	0.35	1.79	(67)

[a]Measurements did not take anisotropy into account.
[b]Measurements did not take nonspecific TMA^+/TEA^+ uptake into account.

4). A reduction in the ECS volume fraction correlates well with growth of blood vessels. The constancy of the tortuosity shows that diffusion of small molecules is no more hindered in the developing brain than in that of the adult. The large ECS channels may allow migration of larger substances (e.g., growth factors) and better conditions for cell migration during development. On the other hand, the large ECS in neonatal brain could significantly dilute ions, metabolites, and neuroactive substances released from cells relative to release in adults and may be a factor in prevention of anoxic injury, seizure, and spreading depression in young individuals. The diffusion parameters could also play an important role in the developmental process itself.

Morphological changes during aging, including cellular loss, loss of dendritic processes, astrogliosis, demyelination, and swollen astrocyte processes are accompanied by changes in the ECS diffusion parameters (36, 44, 68). The α in the cortex, corpus callosum, and hippocampus of senescent rats (aged 26–32 months) is significantly lower than in young adults, e.g., in the cortical layer V ~0.18 instead of 0.21, in the WM ~0.15 instead of 0.19, and in the CA1 pyramidal cell layer of the hippocampus ~0.09 instead of 0.12. Moreover, in hippocampus, the tortuosity λ was significantly higher in CA3 stratum radiatum—1.49 instead of 1.41. It is reasonable to assume that in aging brain there is a significant decrease in ADCs of many neuroactive substances, which accompanies the morphological changes and can contribute to impaired signal transmission, greater susceptibility to anoxia, changes in behavior, and memory impairment.

ECS During Pathological States

Pathological states, e.g., anoxia/ischemia, are accompanied by a lack of energy; seizure activity; excessive release of transmitters and neuroactive substances; neuronal death; glial cell loss or proliferation; glial swelling; production of damaging metabolites, including free radicals; and loss of ionic homeostasis. Others are characterized by inflammation, edema, or demyelination. It is, therefore, evident that they will be accompanied not only by substantial changes in ECS ionic composition (2, 4) but also by various changes in ECS diffusion parameters according to the different functional and anatomical changes.

ECS ionic composition and volume during anoxia/ischemia. Dramatic K^+ and pH_e changes occur in the brain and spinal cord during anoxia and/or ischemia (4, 16, 39, 69). Within 2 min after respiratory arrest in adult rats, blood pressure begins to increase, and pH_e begins to decrease (by ~0.1 pH unit), but $[K^+]_e$ is still unchanged. With the subsequent blood pressure decrease, the pH_e decreases by 0.6–0.8 pH units to pH 6.4–6.6.

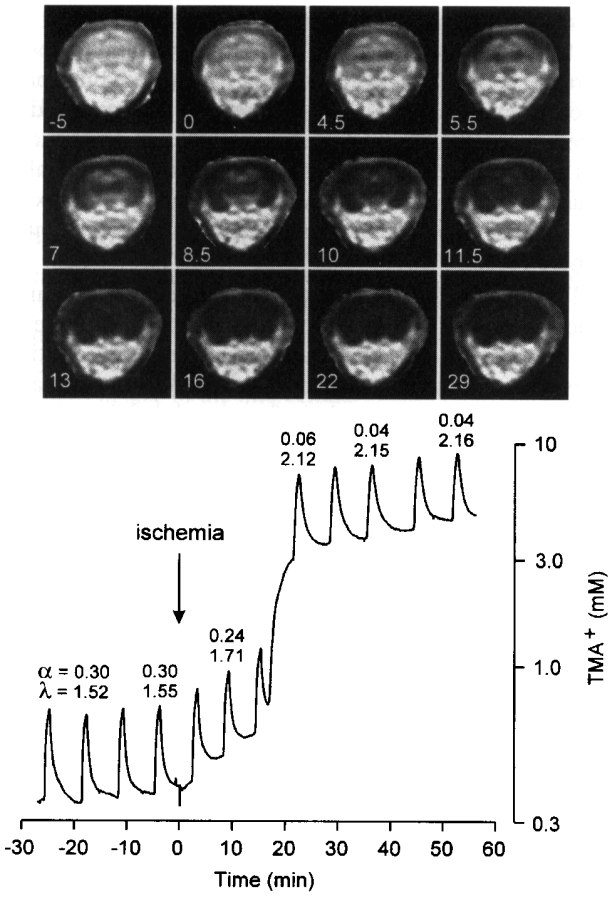

Fig. 7. *Top*, water ADC maps of a 9-day-old rat brain before (*−5*) and at different times after cardiac arrest evoked by intraperitoneal injection of KCl (shown with each record). The maps depict the calculated ADC on a pixel-by-pixel basis. Numbers at lower left corner of images indicate time. The ADC was calculated using diffusion-weighted NMR images obtained with U-FLARE (10 b values ranging up to 1500 s/mm²) and fitting the intensities of corresponding pixels in the images to a Stejskal-Tanner equation (1965). Adapted from (31). *Bottom*, typical TMA^+ diffusion experiment in cortical gray matter (Layer V) of another 9-day-old rat. The TMA diffusion curves were recorded before and during global ischemia. The TMA^+ baseline increases, and the superimposed diffusion curves show an increasing amplitude as ischemia progresses because the scaling is logarithmic. The time after cardiac arrest, α and λ values, are shown with some curves. The time courses of ADC decrease, ECS volume decrease, and tortuosity increase were found to be very similar (31).

This pH_e decrease is accompanied by a steep rise in $[K^+]_e$ to ~50–70 mM; decreases in $[Na^+]_e$ to 48–59 mM, $[Cl^-]_e$ to 70–75 mM, $[Ca^{++}]_e$ to 0.06–0.08 mM, and pH_e to 6.1–6.8; accumulation of excitatory amino acids; slow negative DC potential shift; and a decrease in ECS volume fraction to 0.4–0.7. The ECS volume starts to decrease when the blood pressure drops below 80 mmHg and $[K^+]_e$ rises above 6 mM (39).

During hypoxia and terminal anoxia, the ECS volume fraction in rat cortex or spinal cord decreases from ~0.20 to ~0.04, whereas tortuosity increases from 1.5 to ~2.2 (39, 42). The same ultimate changes were found in both neonatal and adult rats, in grey and white matter, in the cortex, corpus callosum, and spinal cord. However, the time course in white matter was significantly slower than in gray matter, and the time course in neonatal rats was ~10 times slower than in adults (Voříšek and Syková, J Cereb Blood Flow Metab, submitted). This corresponds to the well-known resistance of immature CNS to anoxia. Linear regression analysis revealed a positive correlation between the normoxic size of the ECS volume and the time course of the changes. The slower changes in ECS volume fraction and tortuosity in the nervous tissue during development can contribute to slower impairment of signal transmission, e.g., because of lower accumulation of ions and neuroactive substances released from cells and their better diffusion from the hypoxic area in uncompacted ECS.

In recent studies using diffusion-weighted ^1H MRS/MRI, the apparent diffusion coefficient of water (ADC_W) was measured during terminal anoxia in rats. Anoxia evokes similar decreases in the apparent diffusion coefficient of ADC_W (measured by the NMR method) and ADC_{TMA} (measured by the iontophoretic method and ion-selective microelectrodes). Comparison of ADC_W and ADC_{TMA} in 8–9-day-old rats revealed the same time course, both corresponding to the decrease in ECS volume fraction (Fig. 7) (31). Although water moves freely across the cellular membranes, TMA^+ stays predominantly in ECS. Because the total amount of tissue water is not believed to increase (33), this study (31) shows that changes in ADC of brain tissue water measured by diffusion-weighted in vivo MR techniques predominantly report on extra- and intracellular volume changes resulting from water shift from the extra- to intracellular compartment.

Full recovery to "normoxic" diffusion parameters is achieved after succesful recovery from severe ischemia (39). Beginning 5–10 min after this recovery, the ECS volume fraction significantly increases above the "normoxic" values to an α ~0.30 (Box 4); λ and k' were not significantly different from the values found under normoxic conditions.

The diffusion parameters of the ECS have also been studied in vitro in slices of rat neostriatum during hypoxia (43). Progressive shrinkage of the ECS by ~50% (to α ~0.12), but no significant changes in tortuosity or nonspecific TMA^+ uptake, occurred during exposure to hypoxic media with continual availability of glucose. A study of in vitro ischemia in the slice, involving both the removal of O_2 and glucose, showed that the α of CA1, CA3, and cortex changed from 0.14, 0.20, and 0.18 to 0.05, 0.17, and 0.09, respectively. In contrast, the only change in tortuosity was in CA3, where the λ increased from 1.62 to 1.75 (38). The relatively small increase in extracellular K^+ concentration of ~8 mM in slices (43), which is in contrast to the large K^+ increases

(60–70 mM) observed during hypoxia in vivo, suggests that only mild hypoxia had been evoked and/or that the changes in vivo may be different from those in vitro.

The observed substantial changes in the diffusion parameters during and after progressive ischemia and anoxia in vivo could, therefore, affect the diffusion in ECS and aggravate the accumulation of ions, neurotransmitters, and metabolic substances during ischemia and, thus, contribute to ischemic brain damage. On the other hand, changes in the diffusion parameters may persist long after the ischemic event and affect nonsynaptic transmission in CNS. Changes in the diffusion parameters may also, of course, affect the access to cellular elements of drugs used to treat nervous diseases.

X-irradiation-induced changes in ECS volume and geometry. Radiation therapy is an effective treatment for some human cancers. However, this therapy is limited by radiation injury. Clinical correlates of demyelination and necrosis that occur early include somnolence, changes in intellect, radiation myelopathies, and leucoencepathies. The responses to irradiation of the normal tissue immediately surrounding tumor, which is unavoidably irradiated, are, therefore, of considerable interest. It is generally accepted (70) that radiation injury is caused by mitotic death and depletion of the various cell populations. The main syndromes of radiation injury in the CNS are very similar in rodents and humans. The immature CNS is more sensitive to radiation than the adult nervous system, apparently because of the proliferative potential and increased radiation sensitivity of glial and/or vascular endothelial cells in the developing nervous system (70).

In experiments on the somatosensory neocortex and subcortical white matter of 1-day-old (P1) rats, X-irradiation with a single dose of 40 Gy resulted in radiation necrosis with typical early morphological changes in the tissue—namely, cell death, DNA fragmentation, extensive neuronal loss, blood-brain-barrier (BBB) damage, activated macrophages, astrogliosis, increase in extracellular fibronectin, and concomitant changes in all three diffusion parameters. The changes were observed as early as 48 h after irradiation (at P2-P3) and persisted at P21 (68).

In the nonirradiated cortex, the volume fraction, α, of the ECS is large in newborn rats and diminishes with age (35). X-irradiation with a single dose of 40 Gy blocked the normal pattern of volume fraction decrease during postnatal development and, in fact, brought about a significant increase (68). At P4-P5, α in both cortex and corpus callosum increased to ~0.50. The large increase in α persisted at 3 wk after X-irradiation. Tortuosity, λ, and nonspecific uptake, k', significantly decreased at P2-P5; at P8-P9, they were not significantly different from those of control animals, but they significantly increased at P10-P21. This means that in chronic lesions, e.g., those occuring 1–3 wk after X-irradiation and/or in gliotic tissue, the volume fraction remains elevated, but tortuosity increases. Interestingly, X-irradiation with a single dose of 20 Gy, which resulted in relatively light neuronal damage and loss, as well as BBB damage, did not produce changes in diffusion parameters significantly different from those found with 40 Gy. Less pronounced but significant changes in diffusion parameters were also found in areas adjacent to directly X-irradiated cortex of the ipsilateral hemisphere and the contralateral hemisphere (68).

The observed increase in the extracellular volume fraction in the X-irradiated tissue can also contribute to the impairment of signal transmission, e.g., by diluting ions and neuroactive substances released from cells, and may play an important role in functional deficits, as well as in the impairment of the developmental processes. Moreover, the increase in tortuosity, inferred from the decrease in ADC_{TMA}, in the X-irradiated cortex as well as in the contralateral hemisphere, suggests that even long after mild irradiation, the diffusion of the substances can be substantially hindered. The observed increase in tortuosity seems to be related to astrogliosis, but changes in adhesion molecules or ECM molecules can also account for it.

ECS volume and geometry during inflammation and demylinating diseases. Changes in ECS diffusion parameters can be expected during inflammation during which brain edema may develop. In an experimental model, inflammation was evoked by intracerebral inoculation with a weakly pathogenic strain of *Staphylococcus aureus* (71). There was a lack of changes in water content of the inoculated region, indicating no significant development of brain edema. Acute inflammation and increase in BBB permeability in the abscess region resulted in rather mild changes in ECS diffusion parameters, i.e., volume fraction tended to be somewhat larger, and the tortuosity somewhat smaller.

Dramatic changes in the ECS diffusion parameters were found in the spinal cord of rats during experimental autoimmune encephalomyelitis (EAE), an experimental model of multiple sclerosis (40). EAE, which was induced by the injection of guinea pig myelin basic protein (MBP), resulted in typical morphological changes in the CNS tissue—namely, demyelination, inflammatory reaction, astrogliosis, and BBB damage—and in paraparesis at 14–17 d postinjection of MBP. Paraparesis was accompanied by increases in α in the dorsal horn, in the intermediate region, and in the ventral horn, as well as in white matter, from ~0.18 to ~0.30. There were significant decreases in λ in the dorsal horn and the intermediate region, and decreases in k' in the intermediate region and the ventral horn (40). Although the inflammatory reaction and the astrogliosis preceded and greatly outlasted the neurological signs, the BBB damage had a similar time course. Moreover, changes in ECS diffusion parameters and the manifestation of neurological abnormalities were closely correlated.

These results suggest that the expansion of the ECS alters diffusion parameters in inflammatory and demyelinating diseases, and it may affect the accumulation and movement of ions, neurotransmitters, neuromodulators, and metabolites in the CNS in these disorders, possibly by interfering with axonal conduction.

Unanswered Questions and Prospects

Increasing evidence indicates that the long-term changes in the physical and chemical parameters of the ECS accompany many physiological and pathological states. The question remains, what causes these changes? The changes in size of the intercellular channels are apparently a consequence of cellular (particularly glial) swelling. Abrupt ECS volume decrease may cause "molecular crowding," which can lead to an acute increase in tortuosity. Long-term changes in tortuosity would require changes in ECS composition, either permanent changes in size of the intercellular channels, changes in ECM molecules, or changes in number and thickness of cellular (glial) processes. Available data suggest that in some pathophysiological states, α and λ behave as independent variables. A persistent increase in λ (without decrease in ECS volume) is always found during astrogliosis and in myelinated tissue, suggesting that glial cells can form diffusion barriers and play an important role in diffusion or "volume" transmission. This observation has important implications for our understanding of the function of glial cells.

Changes in ECS ionic composition, size, and geometry may affect

- Synaptic transmission (width of synaptic clefts, permeability of ionic channels, concentration of transmitters, dendritic length constant, etc.);
- Nonsynaptic transmission by diffusion (diffusion of diffusible factors, such as ions, NO, transmitters, neuropeptides, neurohormones, growth factors, and metabolites);
- Neuronal interaction and synchronization;
- Neuron-glia communication;
- ECS ionic homeostasis and glial function;
- Clearance of metabolites and toxic products, and
- Permeability of ionic channels.

The long-term changes in local CNS architecture apparently can result in changes in the efficacy of signal transmission and may underlie plastic changes, LTP or LTD, changes in behavior and memory formation. Hopefully, we will more fully understand all of the consequences of altered ECS in the near future.

Acknowledgments

The contributions of Alexander Chvátal, Tomáš Mazel, Šárka Prokopová, Tamara Roitbak, Zuzana Šimonová, Lýdia Vargová, and Ivan Voříšek are recognized. I thank Charles Nicholson and Alfred Lehmenkühler for continuous discussions concerning diffusion in ECS.

References

1. Nicholson C. Dynamics of the brain cell microenvironment. Neurosci Res Program Bull 1980;18:177–322.
2. Syková E. Extracellular K^+ accumulation in the central nervous system. Prog Biophys Mol Biol 1983;42:135–189.
3. Fuxe K, Agnati LF, editors. Volume transmission in the brain. Novel mechanisms for neural transmission. New York: Raven Press 1991.
4. Syková E. Ionic and volume changes in the microenvironment of nerve and receptor cells. In: Ottoson D, editor. Progress in sensory physiology. Heidelberg: Springer-Verlag 1992;1–167.
5. Bach-y-Rita P. Neurotransmission in the brain by diffusion through the extracellular fluid: a review. Neuroreport 1993;4:343–350.
6. Agnati LF, Zoli M, Strömberg I, Fuxe K. Intercellular communication in the brain: wiring versus volume transmission. Neuroscience 1995;69:711–726.
7. Walz W. Role of glial cells in the regulation of the brain ion microenvironment. Prog Neurobiol 1989;33:309–333.
8. Chesler M. The regulation and modulation of pH in the nervous system. Prog Neurobiol 1990;34:401–427.
9. Deitmer JW, Rose CR. pH regulation and proton signalling by glial cells. Prog Neurobiol 1996;48:73–103.
10. Thomas LB, Steindler DA. Glial boundaries and scars: programs for normal development and wound healing in the brain. NEUROSCIENTIST 1995;1:142–154.
11. Syková E, Rothenberg S, Krekule I. Changes of extracellular potassium concentration during spontaneous activity in the mesencephalic reticular formation ot the rat. Brain Res 1974;79:333–337.
12. Syková E, Preis P, Kříž N. Elevated extracellular potassium concentration in unstimulated spinal dorsal horns of frogs. Neurosci Lett 1985;43:293–298.
13. Singer W. Lux HD. Extracellular potassium gradients and visual receptive fields in the cat striate cortex. Brain Res 1975;96:378–383.
14. Svoboda J, Motin V, Hájek I, Syková E. Increase in extracellular potassium level in rat spinal dorsal horn induced by noxious stimulation and peripheral injury. Brain Res 1988;458:97–105.
15. Johnston BM, Patuzzi R, Syka J, Syková E. Stimulus-related potassium changes in organ of Corti of guinea-pig. J Physiol (Lond) 1989;408:77–92.
16. Syková E, Svoboda J. Extracellular alkaline-acid-alkaline transients in the rat spinal cord evoked by peripheral stimulation. Brain Res 1990;512:181–189.
17. Syková E, Jendelová P, Svoboda J, Sedman G, Ng KT. Activity-related rise in extracellular potassium concentration in the brain of 1–3-day-old chicks. Brain Res Bull 1990;24:569–575.
18. Thomas RC. Ion-sensitive intracellular microelectrodes. Academia London 1978.
19. Syková E. Ion-selective electrodes. In: Stamford J, editor. Monitoring neuronal activity: a practical approach. New York: Oxford University Press 1992;261–282.
20. Vizi ES. Non-synaptic interactions between neurones: modulation of neurochemical transmission. Chichester: Wiley 1984.
21. Nicholson C. Interaction between diffusion and Michaelis-Menten uptake of dopamine after iontophoresis in striatum. Biophys J 1995;68:1699–1715.
22. Nicholson C, Phillips JM. Ion diffusion modified by tortuosity and volume fraction in the extracellular microenvironment of the rat cerebellum. J Physiol (Lond) 1981;321:225–257.
23. Andrew RD, MacVicar BA. Imaging cell volume changes and neuronal excitation in the hippocampal slice. Neuroscience 1994; 62:371–383.
24. Van Harreveld A, Dafny N, Khattab FI. Effects of calcium on electrical resistance and the extracellular space of cerebral cortex. Exp Neurol 1971;31:358–367.
25. Matsuoka Y, Hossmann KA. Cortical impedance and extracellular volume changes following middle cerebral artery occlusion in cats. J Cereb Blood Flow Metab 1982;2:466–474.
26. Korf J, Klein HC, Postrema F. Increases in striatal and hippocampal impedance and extracellular levels of amino acids by cardiac arrest in freely moving rats. J Neurochem 1988;50:1087–1096.

27. Nicholson C, Tao L. Hindered diffusion of high molecular weight compounds in brain extracellular microenvironment measured with integrative optical imaging. Biophys J 1993;65:2277–2290.
28. Benveniste H, Hedlund LW, Johnson GA. Mechanism of detection of acute cerebral ischemia in rats by diffusion-weighted magnetic resonance microscopy. Stroke 1992;23:746–754.
29. Latour LL, Svoboda K, Mitra PP, Sotak CH. Time-dependent diffusion of water in a biological model system. Proc Natl Acad Sci U S A 1994;91:1229–1233.
30. Norris DG, Niendorf T, Leibfritz D. Healthy and infarcted brain tissues studied at short diffusion times: the origins of apparent restriction and the reduction in apparent diffusion coefficient. NMR Biomed 1994;7:304–310.
31. Van der Toorn A, Syková E, Dijkhuisen RM, et al. 1996. Dynamic changes in water ADC, energy metabolism, extracellular space volume and tortuosity in neonatal rat brain during terminal anoxia. Magn Reson Med 1997;36:52–60.
32. Tao L, Vořišek I, Lehmenkühler A, Syková E, Nicholson C. Comparison of extracellular tortuosity derived from diffusion of 3kDa dextran and TMA^+ in rat cortical slices. Soc Neurosci Abstr 1995;21:604.
33. Križaj D, Rice ME, Wardle RA, Nicholson C. Water compartmentalization and extracellular tortuosity after osmotic changes in cerebellum of *Trachemys scripta*. J Physiol (Lond) 1996;492:887–896.
34. Tao L, Nicholson C. Diffusion of albumins in rat cortical slices and relevance to volume transmission. Neuroscience 1996;in press.
35. Lehmenkühler A, Syková E, Svoboda J, Zilles K, Nicholson C. Extracellular space parameters in the rat neocortex and subcortical white matter during postnatal development determined by diffusion analysis. Neuroscience 1993;55:339–351.
36. Mazel T, Roitbak T, Šimonová Z, Brichová H, Harvey A, Syková E. Morphology and diffusion parameters in rat brain during ageing. In: Abstracts of the Second European Meeting on Glial Cell Function in Health and Disease. Arcachon: 1996;61.
37. McBain CJ, Traynelis SF, Dingledine R. Regional variation of extracellular space in the hippocampus. Science 1990;249:674–677.
38. Pérez-Pinzon MA, Tao L, Nicholson C. Extracellular potassium, volume fraction, and tortuosity in rat hippocampal CA1, CA3 and cortical slices during ischemia. J Neurophysiol 1995;74:565–573.
39. Syková E, Svoboda J, Polák J, Chvátal A. Extracellular volume fraction and diffusion characteristics during progressive ischemia and terminal anoxia in the spinal cord of the rat. J Cereb Blood Flow Metab 1994;14:301–311.
40. Šimonová Z, Svoboda J, Orkand P, Bernard CCA, Lassmann H, Syková E. Changes of extracellular space volume and tortuosity in the spinal cord of Lewis rats with experimental autoimmune encephalomyelitis. Physiol Res 1996;45:11–22.
41. Cserr HF, De Pasquale M, Nicholson C, Patlak C, Pettigrew KD, Rice ME. Extracellular volume decreases while cell volume is maintained by ion uptake in rat brain during acute hypernatremia. J Physiol (Lond) 1991;442:277–295.
42. Lundbaek JA, Hansen AJ. Brain interstitial volume fraction and tortuosity in anoxia. Evaluation of the ion-selective microelectrode method. Acta Physiol Scand 1992;146:473–484.
43. Rice ME, Nicholson C. Diffusion characteristics and extracellular volume fraction during normoxia and hypoxia in slices of rat neostriatum. J Neurophysiol 1991;65:264–272.
44. Syková E, Mazel T, Roitbak T. Extracellular space diffusion parameters in the rat brain during ageing. Soc Neurosci Abstr 1996;in press.
45. Bondafeff W, Pysh JJ. Distribution of extracellular space during postnatal maturation of rat cerebral cortex. Anat Rec 1968;160:773–780.
46. Pysh JJ. The development of the extracellular space in neonatal rat inferior colliculus: an electron microscopic study. Am J Anat 1969;124:411–430.
47. Rice ME, Okada Y, Nicholson C. Anisotropic and heterogeneous diffusion in the turtle cerebellum. J Neurophysiol 1993;70:2035–2044.
48. Prokopová Š, Vořišek I, Syková E. Diffusion parameters in myelinated and unmyelinated tissue. In: Abstracts of the Second European Meeting on Glial Cell Function in Health and Disease. Arcachon: 1996;74–75.
49. Bjelke B, England R, Nicholson C, et al. Long distance pathways of diffusion for dextran along fibre bundles in brain. Relevance for volume transmission. Neuroreport 1995;6:1005–1009.
50. Le Bihan D, editor. Diffusion and perfusion. Magnetic resonance imaging. Applications to functional MRI. New York: Raven Press 1995.
51. Stejskal EO, Tanner JE. Spin diffusion measurements: spin echoes in the presence of a time-dependent field gradient. J Chem Phys 1965;42:288–292.
52. Moseley ME, Cohen Y, Mintorovitch L, et al. Early detection of regional cerebral ischemia in cats: comparison of diffusion and T2-weighted MRI and spectroscopy. Magn Reson Med 1993;14:330–346.
53. Le Bihan D, Turner R, Douek P. Is water diffusion restricted in human brain white matter? An echoplanar NMR imaging study. Neuroreport 1993;4:887–890.
54. Jendelová, P, Syková, E. Role of glia in K^+ and pH homeostasis in the neonatal rat spinal cord. Glia 1991;4:56–63.
55. Heinemann U, Lux HD. Ceiling of stimulus-induced rises of extracellular potassium concentration in the cerebral cortex of the cat. Brain Res 1977;120:231–249.
56. Kříž N, Syková E, Vyklický L. Extracellular potassium changes in the spinal cord of the cat and their relation to slow potentials, active transport and impulse activity. J Physiol (Lond) 1975;249: 167–182.
57. Svoboda J, Syková E. Extracellular space volume changes in the rat spinal cord produced by nerve stimulation and peripheral injury. Brain Res 1991;560:216–224.
58. Sontheimer H. Glial neuronal interactions: A physiological perspective. NEUROSCIENTIST 1995;1:328–337.
59. Newman EA. Regulation of extracellular K^+ and pH by polarized ion fluxes in glial cells: The retinal Müller cell. NEUROSCIENTIST 1996;2:109–117.
60. Syková E, Jendelová P, Šimonová Z, Chvátal A. K^+ and pH homeostasis in the developing rat spinal cord is impaired by early postnatal X-irradiation. Brain Res 1992;594:19–30.
61. Jendelová P, Chvátal A, Šimonová Z, Syková E. Effect of excitatory amino acids on extracellular pH in isolated rat spinal cord. In: Abstracts of the 17th Annual Meeting of ENA. Vienna: 1994; 199.
62. Kempski O, Von Rosen S, Weigt H, Staub F, Peters J, Baethmann A. Glial ion transport and volume control. Ann N Y Acad Sci 1991;633:306–317.
63. Walz W, Klimazsevski A, Paterson AI. Glial swelling in ischemia: a hypothesis. Dev Neurosci 1993;15:216–225.
64. Vargová L, Syková E. Effects of K^+, hypotonic solution and excitatory amino acids on diffusion parameters in the isolated rat spinal cord. In: Abstracts of the Annual Meeting of ENA. Amsterdam: 1995;176
65. Chebabo SR, Hester MA, Jing J, Aitken PG, Somjen GG. Interstitial space, electrical resistance and ion concentrations during hypotonia of rat hippocampal slices. J Physiol (Lond) 1995;487: 685–697.
66. Vořišek I, Syková E. Ischemia induced changes in the extracellular space diffusion parameters, K^+ and pH in the developing rat cortex and corpus callosum. J Cereb Blood Flow Metab 1996;in press.
67. Roitbak T, Mazel T, Šimonová Z, Harvey A, Syková E. Extracellular space volume and geometry in rat fetal brain grafts. In: Abstracts of the 2nd Meeting of European Neuroscience. Strasbourg: 1996;in press.
68. Syková E, Svoboda J, Šimonová Z, Lehmenkühler A, Lassmann H. X-irradiation-induced changes in the diffusion parameters of the developing rat brain. Neuroscience 1996:70:597–612.
69. Xie Y, Zacharias E, Hoff P, Tegtmeier F. Ion channel involvement in anoxic depolarisation indused by cardiac arrest in rat brain. J Cereb Blood Flow Metab 1995;15:587–594.
70. Gutin PH, Leibel SA, Sheline GE, editors. Radiation injury to the nervous system. New York: Raven Press 1991.
71. Lo WD, Wolny AC, Timan C, Shin D, Hinkle GH. Blood-brain barrier permeability and the brain extracellular space in acute cerebral inflammation. J Neurol Sci 1993;118:188–193.